STRESSED GE:GA DETECTOR ARRAYS FOR PACS AND FIFI LS

Dirk Rosenthal[a], Jeff W. Beeman[b], Norbert Geis[a], Ullrich Grözinger[c], Rainer Hönle, Reinhard O. Katterloher[a], Stefan Kraft[d], Leslie W. Looney[a], Albrecht Poglitsch[a], Walfried Raab[a], Hilmar Richter[d]

[a]Max-Planck-Institut für Extraterrestrische Physik, Giessenbachstrasse, Postfach 1312, D-85741 Garching, Germany

[b]Lawrence Berkeley National Laboratory, Berkeley, CA 94720

[c]Max-Planck-Institut für Astronomie, Königsstuhl 17, D-69117 Heidelberg, Germany

[d]ANTEC GmbH, Industriestrasse 2, D-65779 Kelkheim, Germany

ABSTRACT

Gallium doped germanium detector arrays in a 16x25 pixel configuration will be used on two future instruments: In the spectrometer section of the Photodetector Array Camera and Spectrometer (PACS) aboard the Herschel satellite and the Field Imaging Far Infrared Line Spectrometer (FIFI LS) aboard the Stratospheric Observatory for Infrared Astronomy (SOFIA). Arrays of slightly stressed Ge:Ga detectors cover a wavelength range from 55 to 105 micron for PACS and from 40 to 120 micron for FIFI LS, whereas arrays of highly stressed Ge:Ga detectors cover a wavelength range from 105 to 210 micron for PACS and 120 to 210 micron for FIFI LS. The entire arrays consist of 25 independent modules of 16 pixels. The detector arrays will be operated with multiplexed integrating amplifiers with cryogenic readout electronics located close to the detector modules. The design of the detector arrays and results of first performance measurements will be reported.

INTRODUCTION

New generations of space and airborne integral field spectrometers require large format arrays of low NEP detectors. In the FIR, photoconductors still offer the higher sensitivity under low background conditions in combination with moderately low operation temperatures (1.7 K to 4 K) when compared to bolometers.

In the 40 to 200 µm range, Ge:Ga photoconductors are commonly used because of their high sensitivity. Ge:Ga photoconductors which are mechanically stressed (~ 700 N/mm^2) in the [100] crystallographic axis are used to cover the wavelength range from 115 to 210 µm[3]. Unstressed Ge:Ga detectors are used to cover the wavelength range from 40 to 115 µm.

The 16x25 pixel detector arrays of stressed Ge:Ga which are described here, will be by far the largest to date. They will be used on two instruments: In the spectrometer section of the *Photodetector Array Camera & Spectrometer* (PACS)[1] aboard the Herschel satellite and the *Field Imaging Far Infrared Line Spectrometer* (FIFI LS)[2] aboard the *Stratospheric Observatory for Infrared Astronomy* (SOFIA).

For both instruments, the integral field concept is realized as illustrated in Fig. 1: A two-dimensional field of view of 5x5 pixels is re-arranged to a one-dimensional slit of 25 pixels, which is fed onto the entrance slit of a conventional long-slit grating spectrograph, dispersed in the perpendicular direction, and imaged onto the detector arrays. One dimension of the detector arrays thereby corresponds to the spatial dimension (25 pixels) and the other to the spectral dimension (16 pixels).

For FIFI LS, this is performed in two spectral channels simultaneously. The blue channel ranges from 42 to 110 µm and the red channel from 110 to 210 µm.

The integral field spectroscopy section of PACS covers the wavelength range from 57 to 210 µm. Both instruments work at a moderate spectral resolution of about 1500 for PACS and 1500 to 5000 for FIFI LS.

Contact information for D. Rosenthal: Email: alpog@mpe.mpg.de, phone +49 89 30000 3293

The entire wavelength range is covered by an unstressed or only slightly stressed Ge:Ga detector array (FIFI LS: 42 to 110 µm; PACS: 57 to 110 µm) and a highly stressed Ge:Ga detector array (110 to 210 µm). The entire spectral range is covered by varying the position of the reflection grating. At a given grating position one or two spectral lines with some continuum are detected.
For the photometry section of PACS, which performs imaging photometry in two channels simultaneously (60-85 µm or 85-130 µm and 130-210 µm), two bolometer arrays of 64x32 pixels (blue channel) and of 32x16 pixels (red channel) will be used.

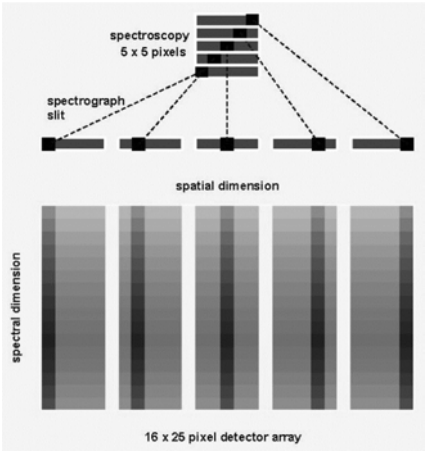

Figure 1: *Integral field concept as it is realized for the PACS integral field spectroscopy section and for FIFI LS. A two-dimensional field of view of 5x5 pixels on the sky is re-arranged by means of an optical image slicer into a one-dimensional slit of 25 pixels which is then fed onto the entrance slit of a conventional long-slit grating spectrograph. Here, the slit is dispersed in the perpendicular direction and imaged onto the detector arrays (lower part). Between each group of 5 spatial pixels is a gap in order to avoid cross-talk of adjacent pixels of the detector array which correspond to non-adjacent positions on the sky.*

ARRAY DESIGN

Module Design

The detector arrays of 16x25 pixels consist of 25 independent modules of 16 pixels each. Due to the high reflectivity and low absorption coefficient of Ge:Ga, each detector is located in an integrating cavity with area-filling light cones to maximize the quantum efficiency. The 16 light cones of one detector module are tilted in the focal plane to match the angle of incoming light from the pupil plane at a distance of 240 mm. The expected dark detector NEP is ≤ $5x10^{-18}$ $WHz^{-1/2}$, which has been reached with a similar design in a balloon-borne experiment[4]. Fig. 2 displays the design of the highly stressed detector module for the PACS and FIFI LS red detector array.

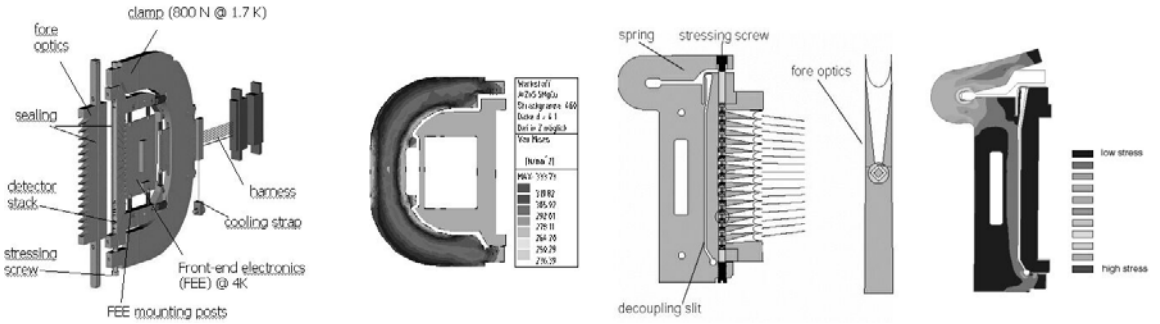

Figure 2: *Schematic of the design of the highly stressed detector module for PACS (left) and FIFI LS(right). For both detector modules the stress to the stack of 16 detector pixels is applied via one stressing screw. A clamp allows a controlled and predictable adjustment of the stress. The detector channel of both arrays are decoupled from the rest of the detector housing to keep the detector channel stress free. This is demonstrated by the result of a finite element analysis (FEA), which is also shown for both detector modules. For the PACS array, the frond-end electronics (FEE) integrated in the U-shaped clamp, whereas for the FIFI LS array the FEE is located at the back-side of the detector module. For both the PACS and the FIFI LS detector arrays, the FEE at a temperature of about 4 K has to be thermally isolated from the housing at a temperature of 1.7 K for the highly stressed array and about 3 K for the low stressed array.*

For both detector modules, a single stressing screw is used to apply the stress to the stack of 16 detectors. A clamp is used to allow a controlled and predictable adjustment of the amount of stress. The detector channels are mechanically decoupled from the rest of the detector module housings in order to avoid any mechanical stress in that part of the housings (see Fig. 2). For the PACS detector module, the front-end electronics (FEE) is integrated in the U-shaped clamp to minimize the length of high impedance wires. For FIFI LS, the FEE is located at the back-side of the detector module housing. In both cases, the FEE at a temperature of ~ 4K has to be thermally isolated from the detector module housing at about 1.7 K for the red arrays and about 3 K for the blue arrays. For PACS this is realized via Kapton posts, whereas the FIFI LS FEE has its own mechanical support and is only weakly coupled via the electrical connections.

Finite Element Analysis

In order to optimize the stressing mechanism, a finite element analysis of a single detector pixel between two cylindrical steel pistons, which apply an external force of 500 N, has been performed.

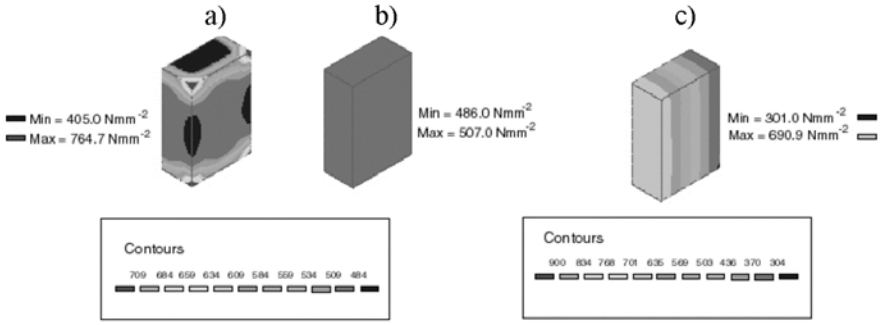

Figure 3: *Results of finite element analysis of one detector pixel between two cylindrical pistons in the case of a perfectly centered (a) and a 20 µm de-centered detector pixel (c) for an external force of 500 N. Displayed is the stress distribution (in N/mm^2) in the direction of the applied force. Also shown is how a pedestal between the pistons and the detector increases the stress uniformity (b).*

The resulting stress distribution is displayed in Fig. 3 for the case of a perfectly centered and a 20 µm de-centered detector pixel. Even in the case of the perfectly centered pixel (Fig. 3a), the distribution of stress values within the detector is very inhomogeneous, with stress values varying between 405 and 765 Nmm^{-2}. This leads to a broadening of the spectral response curve and an enhanced probability of detector breakage. The stress uniformity within one pixel can be significantly improved by using a piston of a material with a higher Young's modulus or pedestals between the pistons and the detector. In our analysis, the use of silver pedestals reduces the variation of stress values to a range of 486 to 507 Nmm^{-2} (Fig. 3b). The range of stress values is drastically increased if the detector is slightly (here: 20 µm) de-centered. Although silver pedestals have been used, the stress values vary between 301 and 691 Nmm^{-2} (Fig. 3c).

Cavity Design

Fig. 4 shows a schematic of one detector pixel in its integrating cavity between the stress pistons for the PACS and the FIFI LS detector arrays. The PACS design uses copper-beryllium pistons with pedestals in order to reach a uniform stress distribution within the pixel (see section before). For the FIFI LS detector array such a pedestal is only used on one side of the detector pixel, whereas on the other side pistons of tungsten carbide with a very high Young's modulus are used. The ball and socket pivot design for both the PACS and FIFI LS detector arrays ensure a compensation of non-parallel surfaces and also a uniform stress distribution along the stack of 16 pixels. For the earlier FIFI 5x5 pixel stressed Ge:Ga detector array, which used cylindrical stress pistons, a stress gradient along the stack of five detector pixels was observed[5]. Electrically, one side of the detector pixel is in contact to the grounded housing and the signal side is on the bias potential for the PACS detector array. In contrast, for the FIFI LS detector array, one side of the detector pixel is in contact with the housing, which is on bias potential, whereas the signal side is on ground potential. The signal ends of the FIFI LS pixels are insulated from the housing by a thin shim of sapphire between the detector pixel and the CuBe pad. Both sides of the PACS pixels are insulated from the housing

by Al_2O_3 plates. The connection of one detector side to the housing is ensured by a wire which is glued to the housing and the respective CuBe pad.

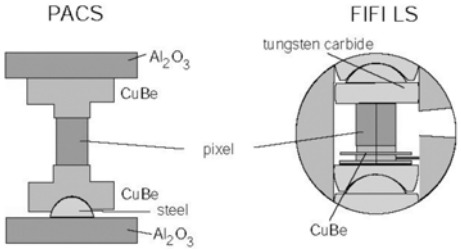

Figure 4: *Schematic of a single detector cavity for the PACS (left) and FIFI LS (right) detector array.*

Cryogenic Readout Electronics

The purpose of the cryogenic readout electronics (CRE), together with some passive components, is to amplify and multiplex the signal of the 16 detectors of one detector module. This is performed by a capacitive feedback transimpedance amplifier (CTIA) for each detector pixel, based on an AC-coupled cascode stage in silicon CMOS technology. The 16 CTIAs with a sample-and-hold-stage are multiplexed on each CRE chip for each detector module. For details of the function and performance of the CRE we refer to the respective paper of this volume[6].

PERFORMANCE

Transient Behavior

Photoconductors usually show a delayed response to a sudden change in the illumination intensity. Characteristic time constants of minutes or hours have been observed under low background conditions. This transient behavior can be distinguished into a fast (of order 10^{-6} sec) and a slow component.

	PACS		FIFI LS	
λ [µm]	P [W]	τ_{slow}[s]	P [W]	τ_{slow}[s]
90	$3x10^{-14}$	0.01	$1.1x10^{-13}$	$3x10^{-3}$
130	$1.5x10^{-14}$	0.016	$4.5x10^{-13}$	$5.5x10^{-4}$
180	$7.5x10^{-15}$	0.023	$1.2x10^{-13}$	$1.5x10^{-3}$

Table 1: *Estimated transient times for the slow component*

The characteristic time τ_{slow} for this slow component is inversely proportional to the photon power received by the detector pixel. Table 1 shows the expected photon background and corresponding time constants for the slow component for three wavelengths for PACS and FIFI LS based on numerical calculations of Haegel[7]. The characteristic times for PACS and FIFI LS are in the 10^{-2} sec and 10^{-3} sec range, respectively. When compared to the expected chopping frequencies of 1 to a few sec^{-1}, this is considered uncritical.
However, these calculations are based on the assumption of an uniform illumination. An inhomogeneous illumination – particularly if the illumination in the region near the contact area of the detector is weaker – can drastically increase τ_{slow}. Therefore, the distribution of incoming light to the detector was simulated by a ray tracing of the light cones. Here, the illumination of the center region of the detector pixel was twice as strong as at the region near the contacts. This is expected to increase τ_{slow} by a factor of about 6 (N. Haegel, priv. comm.), which would still result in acceptable transient times. However, this can be regarded as a worst case since the incoming light will undergo multi-reflections within the integrating cavity, and the distribution of incoming light will be smeared out to some extend.

Responsivity

The upper part of Fig. 5 shows the measured relative spectral responsivity for 6 detector pixels - the first three and the last three with respect to the stressing screw - of one of the highly stressed (top left) and one of the low stressed PACS detector modules. The curves for the different pixels of one detector module are very similar with a very small variation of cutoff wavelengths, which we define as the wavelength > λ_{peak} at which the responsivity is 50% of its peak value.

This shows that no stress gradient along the stack of 16 pixels is present. The lower part of Fig. 5 displays various relative spectral response curves as a function of the applied bias voltage for one of the highly stressed PACS detector modules. The measured cutoff wavelength is increasing for bias voltages from 15 mV to 49 mV from 196 µm to about 205 µm. This behavior may be explained in terms of field assisted photothermal ionization (PTIS)[8] and the Starck effect. The goal for the highly stressed detector module is a cutoff wavelength larger than 200 µm.

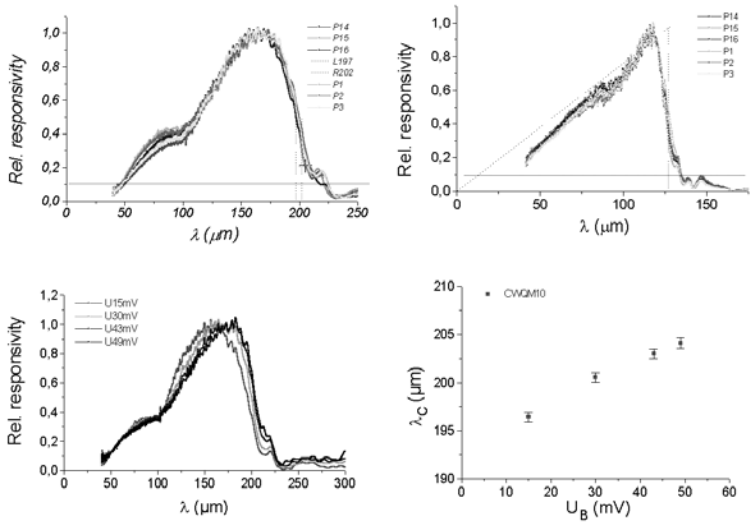

Figure 5: *top: Measured relative spectral responsivity for six pixels of one of the highly stressed detector modules (left) and one of the low stressed detector modules (right). bottom: Measured relative spectral responsivity as a function of the applied bias voltage.*

Quantum Efficiency

More important figure of merits than the responsivity are the noise equivalent power (NEP) and the quantum efficiency (QE) since they determine the actual sensitivity of the detection system. Since the knowledge of these quantities was urgently needed and there was no working CRE available, a conventional transimpedance amplifier (TIA) was used to determine the QE for one of the highly stressed

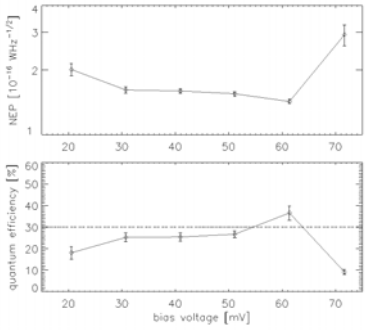

Figure 6: *Averaged results of 22 individual measurements with a photon power of 1x10^{-12} W and at detector module temperature of about 1.9 K. Displayed is the measured noise equivalent power (NEP) and the derived quantum efficiency (QE) as a function of the applied bias voltage. The quantum efficiency can be derived from the measured NEP under the assumption of background limited performance.*

detector modules. To have the actual amplifier at room temperature outside the cryostat, heated JFETs (T~50 K) integrated in the U-shaped clamp of the PACS detector module (see Fig. 2) had to be used to convert the high impedance of the detector signal to a lower value. To avoid any photon background due to the thermal radiation of the JFETs, they had to be enclosed in a light tight box, which is thermally isolated from the detector module housing at a temperature of about 1.8 K. Feedback resistors, at the temperature of the detector module housing, with a room temperature resistance of 3 and 10 GΩ were used. The measured signal is the bias voltage times the ratio of the feedback and the detector resistance. Fig. 6 shows the averaged result from 22 individual measurements of the NEP and the QE with a photon power of 1x10^{-12} W and at a detector module temperature of about 1.9 K as a function of the applied bias voltage. For bias voltages smaller than 30 mV, the measurements are still dominated by the readout noise, whereas for bias voltages larger than the breakdown voltage of 60 mV, the noise due to the avalanche effect starts to dominate. From the almost independence of the NEP from the bias voltage and from comparison of the

measured NEP at various photon powers, the measurements are thought to be almost limited by the noise of the photon background in the intermediated bias voltage range from 30 to 60 mV.
The bottom of Fig.8 displays the QE, which can be derived from the measured NEP under the assumption of background limited performance. The QE efficiency increases from 25% at a bias voltage of 30 mV to 36% at a bias voltage of 60 mV. The requirement of 30% is therefore met. The value of 36% may even be regarded as a lower limit of the QE since the QE increases, as the NEP decreases, slightly with bias voltage until the bias voltage exceeds the breakdown voltage of 60 mV. This can be a hint that the measurement is not quite background limited and there is still some non-negligible contribution of the readout noise.

STATUS AND FUTURE PROSPECTS

The status for the PACS Ge:Ga detector arrays can be summarized as follows:

- All 24 qualification models – 12 for the blue and 12 for the red array – are assembled and tested for the relative spectral response
- The cryogenic environmental testing consisting of a thermal cycling test and a cryovibration test has been successfully performed on two of the qualification models. For the cryovibration test the maximum load levels were 20 g for sine excitation and 12 g rms for random excitation.
- The next steps in the performance test sequence, the spectral calibration and glitch investigation, are in preparation.
- The design of the detector modules has been finalized and the assembly of flight models started.

The status summary for the FIFI LS detector arrays is:

- The entire red array of 25 detector modules plus two spare detector modules has been assembled
- The blue detector array for FIFI LS is still under development.

Future integral field spectrometers will require ever larger two-dimensional FIR detector arrays to further increase the observation efficiency. The principle for the detector arrays presented here allows an almost arbitrarily expansion of the array size in one dimension, i.e. increasing the number of detector modules. This is only limited by optical requirements (area which can be illuminated) or by increased costs. An increase in this dimension could be useful to increase the simultaneously detected spectral range for a fixed number of spatial pixels in order to detect for example faint objects of unknown red-shift.
In the other dimension, means the number of pixels within one detector module, an increase of about a factor of 2 seems feasible. Even though an expansion in the total pixel number by a factor of up to 10 seems technically possible, such an expansion would dramatically increase the total costs.
Therefore, it is strongly desirable to find alternative solutions. Such an alternative could be the development of sufficiently sensitive monolithic GaAs detector arrays of blocked impurity band (BIB) detectors. Such arrays might offer the possibility to manufacture large FIR detector arrays combined with the advantage of an extended wavelength coverage up to ~ 310 μm without the need of a mechanical stress application at moderately low operating temperatures of about 1.7 K[9,10].

REFERENCES

1. A. Poglitsch, C. Waelkens, & N. Geis in The Promise of the Herschel Space Observatory, Proc. Symposium, eds. G.L. Pilbratt, J. Cernicharo, A.M. Heras, T. Prusti, & R. Harris, ESA SP-460, 29 (2001)
2. L.W. Looney, N. Geis, R. Genzel, W.K. Park, A. Poglitsch, W. Raab, D. Rosenthal, & A. Urban, SPIE vol. 4014, 14 (2000)
3. A.G. Kazanskii, P.L. Richards & E.E. Haller, Appl. Phys. Lett. 31, 496 (1977)
4. N. Hiromoto, T. Itabe, T. Argua, H. Okuda, H. Matsuhara, H. Shibai, T. Nakagawa, & T. Saito, IR Phys., 29, 255 (1989)
5. G.J. Stacey, J.W. Beeman, E.E. Haller, N. Geis, A. Poglitsch & M. Rumitz, Int. J. Inf. Mill. Wav., 13, 1689 (1992)
6. Y. Creten, P. Merken, J. Putzeys, & C. Van Hoof, 3-10 this volume (2002)
7. N.M. Haegel, PACS internal report PACS-ME-TN-011
8. E.E. Haller & W.L. Hansen, Adv. In Phys., 30, 93 (1981)
9. R. Katterloher, G. Jakob, M. Konuma, N.M. Haegel, & E.E. Haller, 3-41 this volume (2002)
10. E.E. Haller & J.W. Beeman, 2-06 this volume (2002)